Orientation dependence in the reaction of Xe* with photodissociation polarized IBr

Mattanjah S. de Vries, Vojislav I. Srdanov, Ciaran P. Hanrahan, and Richard M. Martin

Citation: The Journal of Chemical Physics **78**, 5582 (1983); doi: 10.1063/1.445438
View online: http://dx.doi.org/10.1063/1.445438
View Table of Contents: http://scitation.aip.org/content/aip/journal/jcp/78/9?ver=pdfcov
Published by the AIP Publishing

Orientation dependence in the reaction of Xe* with photodissociation polarized IBr

Mattanjah S. de Vries, Vojislav I. Srdanov, Ciaran P. Hanrahan, and Richard M. Martin

Department of Chemistry, University of California, Santa Barbara, California 93106
(Received 3 August 1982; accepted 18 November 1982)

The reaction of metastable Xe* with IBr to produce XeI* and XeBr* excimers was studied in crossed molecular beams. The IBr beam was rotationally polarized by using laser photodissociation to selectively remove most of the M state distribution. The reaction cross section was found to be largest when the Xe* approaches parallel to the plane of rotation of the IBr, and smallest when the Xe* approaches perpendicular to the plane of rotation. Reaction models for excimer formation are discussed, and it is concluded that the observed steric effect results from the anisotropy of the ionic $Xe^+/IBr^-(^2\Pi)$ potential surface, involving the first excited state of IBr^-, which is the intermediate state in the formation of XeI*.

I. INTRODUCTION

Molecular collision processes have been studied in crossed molecular beam experiments as a function of many parameters. However, the study of the dependence upon molecular orientation has been limited to only a few systems. Clearly both reactive and nonreactive molecular dynamics depend upon the approach geometry, but this parameter is generally the most difficult one to control experimentally.

A limited number of polar molecules have been polarized by hexapolar fields.[1] Another approach has been the use of optical excitation to obtain polarized excited atoms,[2] excited molecules,[3] and molecular ions.[4] With this technique, excited molecules will, at best, have a spatial distribution of the form $\cos^2\theta$, where θ is the angle between the light vector and the angular momentum vector. As the transition is saturated, the polarization of the excited species decreases, while the remaining ground state molecules in the relevant rovibrational levels become highly polarized. Therefore, sharp polarizations of ground state molecules can be obtained by exciting most of the sample to a dissociative continuum. The theory of molecular polarization by selective photodissociation was first given by Zare[5] and Bersohn and Lin.[6] Ling and Wilson[7] extended the theory and demonstrated the polarization of IBr using photofragment spectroscopy. We have, for the first time, used this concept to study the effect of molecular polarization on reactivity in a crossed beam experiment.[8]

IBr molecules in a beam were polarized by selective photodissociation. A beam of metastable Xe* crossed the IBr beam giving the xenon halide excimers,

$$Xe^* + IBr \rightarrow XeBr^* + I \tag{1a}$$

$$\rightarrow XeI^* + Br\ . \tag{1b}$$

The effect of IBr polarization on the reaction cross section was observed by monitoring the intensity of excimer emission as a function of the direction of polarization of the photodissociation laser. The Xe*/IBr system was chosen to demonstrate the feasibility of this technique because both the photodissociation of IBr[7,9,10] and its reaction with metastable rare gases[11] have been well studied. The cross section for reaction (1) is very large due to the harpoon mechanism, which involves curve crossings at large internuclear distance.

II. PRINCIPLE OF THE EXPERIMENT

The absorption probability for a dipole transition is proportional to $|\mu|^2|\epsilon|^2\cos^2\eta$, where η is the angle between the light vector $\bar{\epsilon}$ and the transition dipole moment $\bar{\mu}$. For symmetry reasons, the latter is fixed with respect to the molecular frame. Restricting ourselves to diatomic molecules, $\bar{\mu}$ will be parallel to the intermolecular axis when the electronic angular momentum does not change ($\Delta\Lambda = 0$), and perpendicular to the intermolecular axis when $\Delta\Lambda = 1$. Molecules with different orientations will have different absorption probabilities, and therefore, different rates of dissociation. In this work the light pulse is long compared to the molecular rotational period, which means that the absorption probability depends only on the angle between the light vector and the plane of rotation of the molecule. This implies a different rate of dissociation for different orientations of the angular momentum vector J with respect to the light vector. Quantum mechanically, this means that different M states are depleted at different rates, where M is the projection of $\bar{J}$ on $\bar{\epsilon}$. Therefore the molecules that remain after photodissociation have an anisotropic M state distribution, with the degree of anisotropy increasing with the intensity of the light pulse. For high J values and a parallel transition, it is, in principle, possible to photodissociate essentially all molecules except those rotating in a plane perpendicular to the light vector, i.e., those with $M = \pm J$. The fraction of molecules in a certain (M, J) level that remain undissociated can be written as[7]

$$\frac{N_f}{N_0} = \exp[-3\sigma F(S_P^2 + S_Q^2 + S_R^2)]\ , \tag{2}$$

where F is the number of photons/cm^2 pulse, σ is the total absorption cross section for the relevant transition, and the S terms are the line strengths for the different rotational branches. The latter are a function of M and J and are different for a parallel vs a perpendicular transition. Figure 1 shows the behavior of Eq. (2) for several cases. The highest degrees of polarization are obtained for pure parallel transitions and high values of σF. In practice, there is a tradeoff between the de-

 0021-9606/83/095582-08$2.10

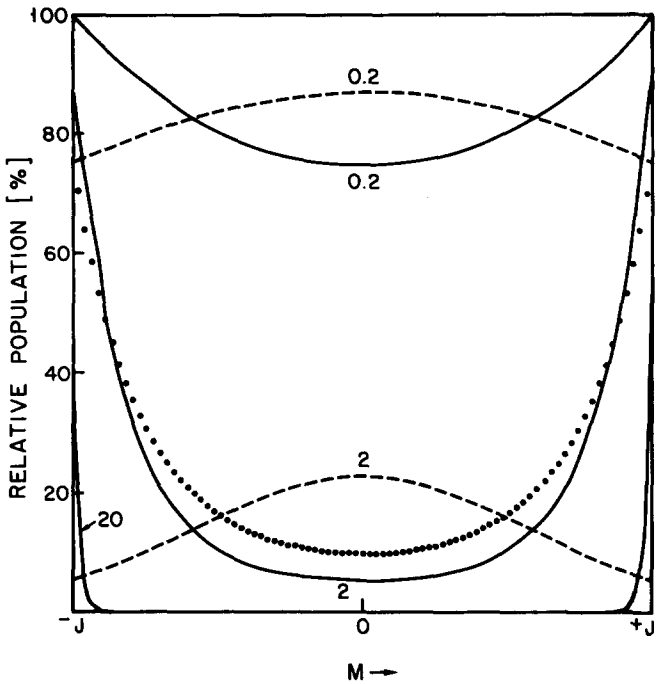

FIG. 1. Relative M state populations ($J=43$) following a laser pulse. The product of flux and cross section (σF) is indicated for each curve. Solid curves refer to parallel transitions, and broken curves to perpendicular transitions. The dotted curve is calculated for the experimental conditions of this work, i.e., $\sigma F = 1.6$ and a 90% parallel transition. See Ref. 7 for a discussion of the computational method.

gree of polarization and the beam intensity, i.e., the fraction of molecules left. For example, a high degree of polarization is obtained with $\sigma F = 1.6$, while more than 20% of the molecules remain undissociated. For IBr these conditions are easily met. IBr has an absorption continuum that peaks near the second harmonic line of a Nd-YAG laser (532 nm). At that wavelength the transition is of 90% parallel character with a total absorption cross section of 8.1×10^{-19} cm^2.

III. EXPERIMENTAL METHOD

The experimental setup is shown in Fig. 2. The Xe beam emerged from a supersonic nozzle source in a differentially pumped source chamber, and passed through a skimmer into the crossed beam chamber. The Xe beam then passed through a cold cathode discharge which excited a small fraction to the metastable $^3P_2$ and $^3P_0$ levels. Other excited states are either very short lived, or were removed by sweeper plates downstream, which also served to remove ions. The metastable atoms were monitored by measuring the current of electrons emitted when the atoms struck a gold surface in a Faraday cage detector. The Xe* beam was crossed at right angles by an effusive IBr beam from a multichannel capillary array. A liquid nitrogen cooled baffle with a slit was used to form a collimated IBr beam and condense the remainder of the beam so as to minimize background IBr in the interaction region. Both beams had rectangular cross sections of about 2×5 mm in the interaction region. XeBr* and XeI* chemiluminescence was detected perpendicular to the IBr beam and at an angle of 60° with respect to the Xe beam. The light was collected with a 50 mm quartz lens and passed through a Corning 7-54 absorption filter to an EMI 9750 photomultiplier tube. Due to the wavelength response of the filter/phototube combination the detection efficiency increased between 200 and 400 nm, and was therefore larger for XeBr* than for XeI*. The filter was used to minimize the amount of background radiation from the discharge entering the photomultiplier tube. A pulsed 532 nm beam from a frequency doubled Nd-YAG laser intersected the IBr beam slightly above the interaction region. The laser beam was orthogonal to the particle beams. The light was linearly polarized and the light vector could be rotated by a half-wave plate. The laser was focused onto a pinhole in front of the interaction region for spatial filtering to prevent blinding of the photomultiplier. The laser beam diameter was 5 mm at the intersection with the IBr beam, so as to insure good overlap. The XeBr* and XeI* excimers have short lifetimes, of the order of 10 ns,[14] and therefore the fraction escaping the interaction region before detection was negligible. The laser beam was pulsed at 10 pps, with a pulse duration of 10 ns, and the time dependence of excimer emission following each pulse was monitored using photon counting techniques and a multiscalar system with time channel widths of 1.2 μs.

IV. RESULTS

Figure 3 shows the excimer emission intensity as a function of time after the laser pulse. The broken line indicates the chemiluminescence intensity with the laser off and the particle beams on, and includes the chemiluminescence from collisions of Xe* with background IBr. The laser pulse depletes the IBr beam in and just before the Xe* interaction region. As this dip in the IBr beam intensity moves through the Xe* beam, the excimer emission decreases to a minimum at about 5 μs and then increases back to the dc level as the dip exits the interaction region.

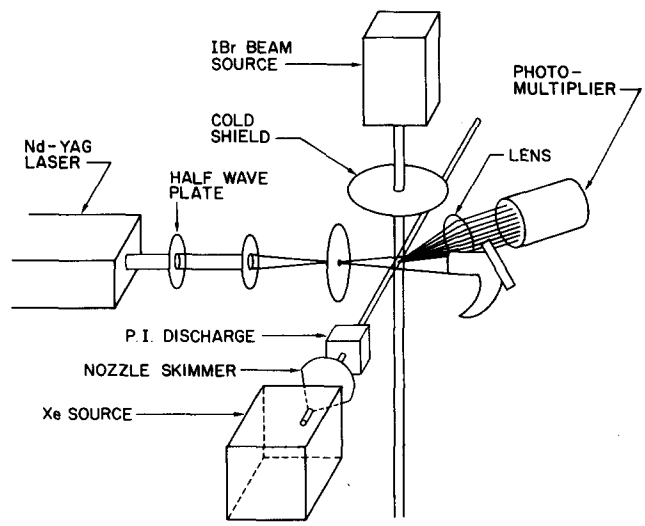

FIG. 2. Schematic diagram of the experiment.

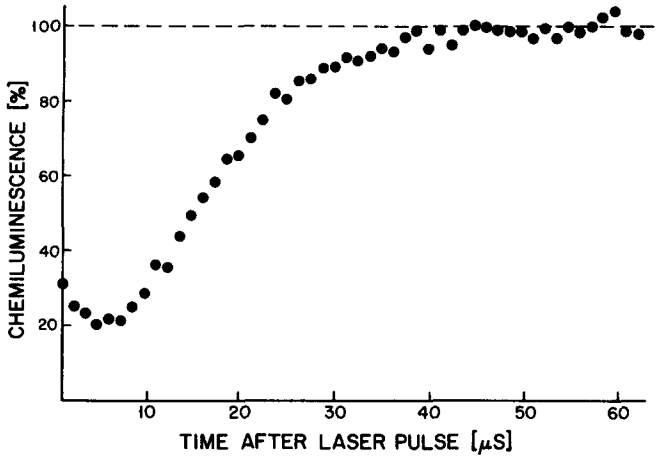

FIG. 3. Chemiluminescence signal as a function of time after the laser pulse, with background chemiluminescence subtracted. Broken line indicates dc level with laser off.

The energy of the 532 nm light is not sufficient to ionize Xe($^3P_2$, $^3P_0$) by a one-photon transition, but the laser radiation could possibly excite one or both of the metastables to higher states which could be ionized by a second photon. To check this possibility the laser beam was translated with respect to the Xe* and IBr beams. No effect was observed when the laser beam intersected the Xe* beam in front of the IBr beam. As an additional check of the method, the same experiment was performed with Br_2, which has an absorption coefficient seven times smaller than IBr at 532 nm. With the same Br_2 beam density, the relative dip in the excimer emission was about seven times smaller than with IBr, showing that the observed effect was due to halogen photodissociation and not to removal of Xe($^3P_2$, $^3P_0$).

Ideally one would like to employ a laser beam with a uniform intensity over the molecular beam interaction region. Unfortunately, the laser beam used in these experiments had shaded rings or "fringes," i.e., concentric circles where the power was relatively low. The IBr molecules in these fringe regions were illuminated with less than the intensity needed to achieve a high degree of alignment. In other words, neither absorption nor alignment were uniform in space. Therefore the degree of IBr polarization that was achieved could only be roughly estimated, by estimating the degree of saturation of the absorption. Figure 4 shows a plot of the percent decrease in chemiluminescence ($100\ \Delta I/I_0$) as a function of laser power. The measured points were obtained from plots such as Fig. 3. I_0 is the dc signal obtained by averaging ten channels starting after 60 μs, I is the average signal in the first ten channels, and $\Delta I = I_0 - I$. In the high power areas of the laser beam the fraction N/N_0 of IBr molecules remaining is $e^{-\sigma F}$. This follows from the time dependent rate equation

$$\frac{dN}{dt} = -\sigma \Phi N , \tag{3}$$

where Φ is the photon flux (photons/cm^2 s). Integration over time during the pulse duration Δt yields:

$$N = N_0 \exp\left[-\sigma \int_0^{\Delta t} \Phi(t)\, dt\right] = N_0 \exp(-\sigma F) . \tag{4}$$

Therefore, the fractional depletion is $1 - e^{-\sigma F}$. As a crude first approximation we assume that a fraction f of the molecules were in the high intensity laser field, while the other molecules were not affected by the laser at all, i.e., the spatial distribution of the laser intensity is approximated by a step function. The relative chemiluminescence decrease is then given by

$$\frac{\Delta I}{I_0} = f(1 - e^{-\sigma F}) . \tag{5}$$

This model was found to fit the data better than the assumption of a uniform laser intensity ($f = 1$). The solid curve in Fig. 4 was obtained with $f = 0.55$, and shows that the transition is becoming saturated at the higher power levels. Without saturation the signal decrease would be linear, as shown by the broken line.

The residual chemiluminescent signal I/I_0 was measured as a function of polarization angle using pulses of 740 mJ/cm^2, giving an average σF value of 1.6 in the high intensity region, and the corresponding M state distribution shown in Fig. 1. The light vector was rotated by means of a half wave plate in 30° steps, accumulating data at each angle. The procedure was repeated many times in order to eliminate possible long term drift effects, and the laser power was checked periodically. The result of such a scan is shown in Fig. 5. The dashed line is a least-squares fit to the data of the form

$$\frac{I}{I_0} = A \sin(\theta_{\text{lab}} + \Phi) = A \sin \theta_{\text{c.m.}} , \tag{6}$$

where θ_{lab} is the laboratory angle between the light vector (which is in the cross beam plane) and the Xe* beam, and Φ is the center-of-mass coordinate system correction to give the angle $\theta_{\text{c.m.}}$ between the light vector and the most probable Xe* + IBr relative velocity vector. As shown in Fig. 5, the chemiluminescence is largest when $\theta_{\text{c.m.}} = 90°$ and smallest when $\theta_{\text{c.m.}} = 0°$.

The above conclusion is true only if the variation in

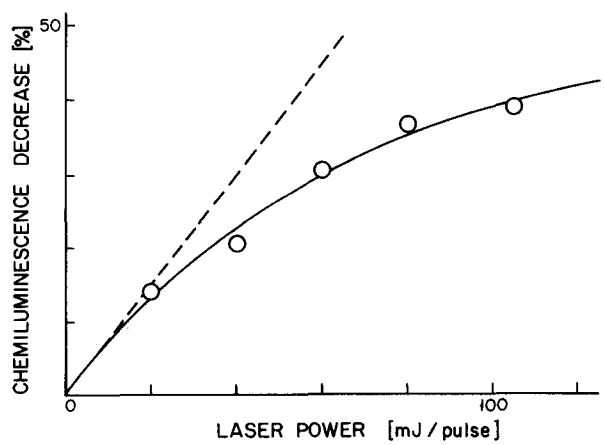

FIG. 4. Total chemiluminescence signal decrease as a function of laser power (background not subtracted). See the text for discussion of the calculated curve.

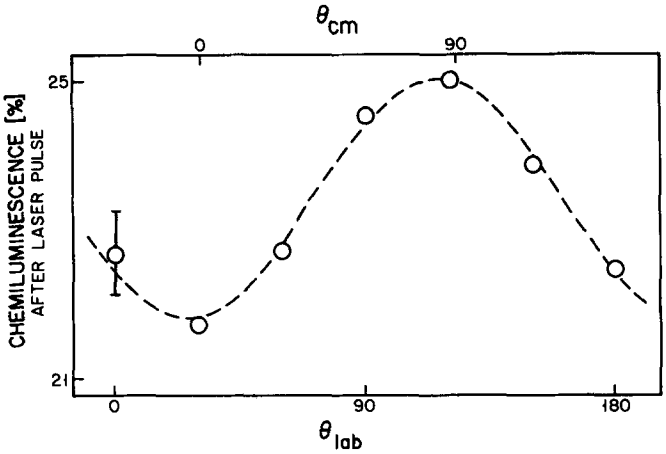

FIG. 5. Chemiluminescence after the laser pulse as a functio of the angle θ_{lab} between the light vector and the Xe* beam. The angle $\theta_{c.m.}$ between the light vector and the most probable Xe* + IBr relative velocity vector is indicated on the top scale. The error bars are given by the standard deviations in the number of counts for each data point. A typical error bar is shown at the left.

excimer emission intensity is a cross section effect and not a result of anisotropic emission from polarized excimers. If the polarized angular momentum J of the IBr was transformed to polarized angular momentum J' of the excimers, then rotation of $\bar{\epsilon}$ in the cross beam plane would cause rotation of J' in that plane. In that case the emission would be anisotropic with respect to the laboratory frame, rather than with respect to the center of mass frame. The angular distribution would depend on the character of the transition, which in this case is parallel, i.e., $\Delta\Omega = 0$.[15,16] Analysis of the emission profile shows[17] that this would lead to a maximum and minimum in the emission with the light vector parallel ($\theta_{lab} = 0°$) and perpendicular ($\theta_{lab} = 90°$) to the Xe* beam, respectively. This is clearly in contradiction with the results of Fig. 5, showing that the variation in excimer intensity is a cross section effect rather than a result of anisotropic emission. It is also interesting to examine whether the transference of polarized reactant angular momentum to product angular momentum would be expected to give strong polarization of the excimers in the Xe*/IBr system. The most extreme such case would be in the limit of zero orbital angular momentum, where the excimer angular momentum polarization would be equal to the IBr angular momentum polarization. However, as will be discussed below, these are harpoon-type reactions, in which the initial orbital angular momentum can be as large as 250 $\hbar$, while the average IBr angular momentum is of the order of 40 $\hbar$. Hennessy and Simons[18] have measured the polarization of the XeBr* excimer emission from the similar reaction of Xe* with Br_2 in crossed molecular beams. They find that even at thermal velocities the transfer of orbital angular momentum to product angular momentum is important, giving significant excimer polarization. Apparently transformation of orbital angular momentum into product angular momentum is the main effect causing excimer polarization, and therefore the IBr angular momentum distribution is not expected to have a strong effect on the excimer angular momentum distribution.

The geometry of photodissociation aligned diatomic molecule collisions is illustrated for parallel electronic transitions in Fig. 6. For a parallel transition near saturation only molecules with M states close to $\pm J$ remain (see Fig. 1), i.e., molecules which are rotating in planes nearly perpendicular to $\bar{\epsilon}$. The results of Fig. 5 show that the reaction probability is largest for $\bar{v}_{rel}$ parallel to the plane of rotation and smallest for $\bar{v}_{rel}$ perpendicular to the plane of rotation. When drawing conclusions from this, it should be remembered that there is a wide range of reactive impact parameters. The implications of this are discussed below.

V. DISCUSSION

The reactions of metastable rare gas atoms with halogen molecules are analogous to those of the alkali/halogen systems.[19] At a large internuclear distance R_c the covalent Xe* + IBr potential crosses the ionic $Xe^+ + IBr^-$ potential, and an electron jump can take place. At thermal velocities, when the system follows the ionic potential the reaction takes place with unit probability. The relevant potential curves are sketched in Fig. 7. Two ionic curves are indicated, surface I correlating with ground state $IBr^-(^1\Sigma^+)$ and surface II correlating with excited state $IBr^-(^2\Pi)$. For the sake of clarity only

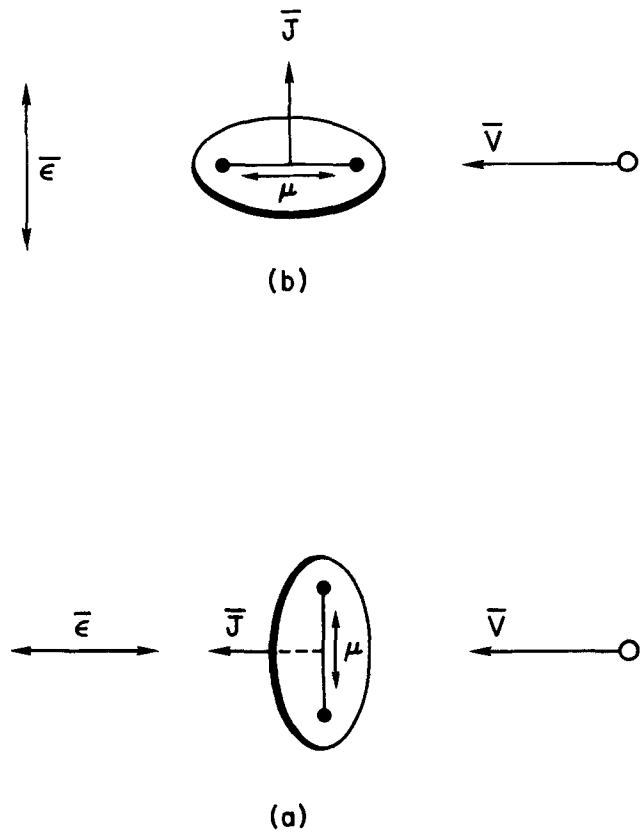

FIG. 6. Geometry of photodissociation polarization for parallel transitions: (a) Perpendicular approach to the plane of rotation; (b) Parallel approach to the plane of rotation.

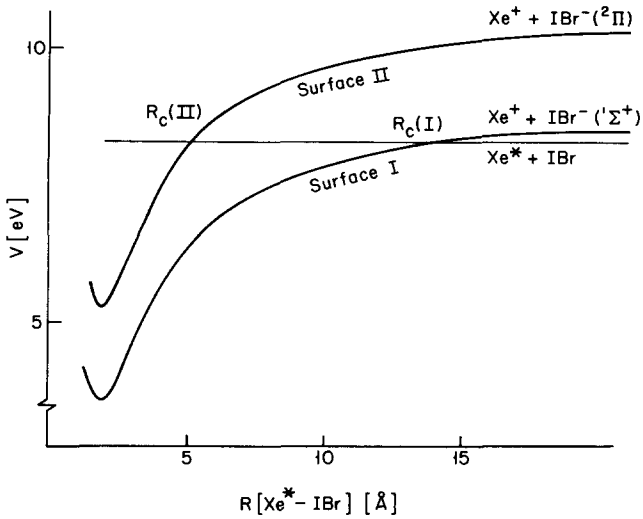

FIG. 7. Schematic potential energy diagram for the Xe–IBr system. Surface involving the $Xe(^3P_2)$ and $Xe^+(^2P_{3/2})$ states are shown. See the text.

one of the $^3P_{2,0}$ metastable states and one of the $^2P_{1/2,3/2}$ rare gas ion states is shown. Ground state IBr^- dissociates into $I + Br^-$, while excited state IBr^- dissociates into $I^- + Br$. This means that surface I is the intermediate in formation of XeBr while surface II leads to formation of XeI. There are two possible ways to reach surface II: (i) a curve crossing between the covalent surface and surface II; or (ii) a coupling between surface I and surface II.

A. Electron transfer probabilities

We will first consider the electron jump probability P_c, which is given by the Landau–Zener formula:

$$P_c = 1 - \exp\left[\frac{-2\pi H_{12}^2(\alpha)}{h\Delta V v_{\mathrm{rel}}}\right] . \tag{7}$$

Here ΔV is the difference in potential slopes, v_{rel} is the relative velocity at R_c, and $H_{12}(\alpha)$ is the coupling matrix element. The latter is a function of α, the angle between the molecular axis and the line connecting the center of mass of the molecule with the atom at the crossing distance R_c. This angular dependence is usually expressed in the form[19]

$$H_{12,}(\alpha) = H_{12} f(\alpha) . \tag{8}$$

It comes about because the electron jump is only allowed when both potential surfaces have the same symmetry, which is not necessarily the case in every orientation. The two symmetry groups involved in this case are $C_{\infty v}$ for the collinear conformation and C_s for all others. (For a homonuclear diatomic C_{2v} would indicate broadside attack.) Table I summarizes the symmetries of the relevant potential surfaces. It follows from the table that the electron jump to the $^2\Pi$ state of the negative ion is forbidden in the collinear conformation. These correlations must be viewed with some reservations because there is large spin-orbit coupling and therefore Σ and Π are not good quantum numbers. On the other hand the same conclusions are reached when the metastable is replaced by an alkali.[12] This is very reasonable since the core hole should not influence the behavior of the outer electron at large internuclear distances. Indeed there is detailed experimental evidence showing the similarities between alkali/halogen and metastable rare gas/halogen systems.[11,20] We therefore adopt the same forms for $f(\alpha)$ that have been found to hold in the alkali/halogen systems,[13,21] i.e., $f(\alpha) = 1$ for the crossing with surface I and $f(\alpha) = \sin(\alpha)$ for the crossing with surface II.

It is difficult to estimate the coupling matrix elements without exactly knowing the electron affinities of the halogen molecule. Using Olson's rules[22] and a reactive E.A. of 2.45 eV,[23,24] determined from alkali reaction studies, we find that the first crossing between the $^3P_2$ surface and surface I could be as far out as 11 Å. At this distance H_{12} will be extremely small and therefore $R_c(I)$ could be passed diabatically by a significant fraction of the trajectories. This situation is unique for Xe since its metastables have a relatively low ionization potential. On the other hand the E.A. to form $IBr^-(^2\Pi)$ is of the order of 1 eV. Therefore, the crossing with surface II is at about 5 Å and is strongly avoided. In this case H_{12} is of the order of 0.5 eV. As a result we find that P_c is always near unity, except when α approaches zero, causing P_c to vanish.

In the following discussion we consider two models which can explain the observed steric effect. The first model assumes that the reaction occurs via surface I. Since the cross section for electron transfer to surface I is not expected to be orientation dependent, the total reaction cross section should not have a steric effect with this model. However the branching ratio for formation of XeI* vs XeBr* may be orientation dependent, giving the observed effect. This model is discussed in Sec. V B. The second model assumes that essentially all trajectories pass $R_c(I)$ diabatically, i.e., follow the neutral curve. The cross section for transfer to surface II is expected to be strongly orientation dependent, and this would result in the type of steric effect observed experimentally. The second model is discussed in Sec. V C.

TABLE I. Symmetries of the relevant potential surfaces in the Xe*/IBr system[a].

	Xe* + IBr	$C_{\infty v}$	C_s
Covalent	$^3P_2 + {}^1\Sigma^+$	$^3\Pi_2$	$^3A', {}^3A''$
Surface	$^3P_0 + {}^1\Sigma^+$	$^3\Pi_{0^+}, {}^3\Pi_{0^-}$	$^3A', {}^3A''$
Surface I	$^2P_{3/2} + {}^2\Sigma^+$	$^3\Pi_2$	$^3A', {}^3A''$
	$^2P_{1/2} + {}^2\Sigma^+$	$^3\Pi_{0^+}, {}^3\Pi_{0^-}$	$^3A', {}^3A''$
Surface II	$^2P_{3/2} + {}^2\Pi$	$^3\Delta_3, {}^3\Sigma_1$	$^3A', {}^3A''$
	$^2P_{1/2} + {}^2\Pi$	$^3\Pi_1, {}^3\Sigma_1$	$^3A', {}^3A''$

[a]Singlet states derived from the ion pairs are omitted, since they cannot couple to the triplet covalent states. Also states involving a p_σ core hole in the Xe ion or atom are omitted, because for the covalent states that would correlate with the $^3P_1$ atom.

B. Model I: Oreientation dependence of the XeI*/XeBr* branching ratio

As discussed earlier, surface I correlates with XeBr* and surface II correlates with XeI*. In model I we assume that all reactive trajectories follow surface I initially, and that the subsequent coupling to surface II is orientation dependent. This problem was discussed in a general way by Kwei and Herschbach,[26] and was subsequently considered by Balin-Kurti in his quantum mechanical calculations for the $Li+F_2$ system.[27] For this system he found that surface II is always above surface I, except when the Li atom is in between the F atoms, in which case the surfaces become degenerate. This linear configuration (I-Xe-Br in our system) occurs for small impact parameter collisions and broadside attack. For the alkali/halogen systems there is much evidence in support of this model, as discussed by Gislason.[28]

The application of this model to explain the observed steric effect is illustrated in Fig. 8. The total reaction cross section is independent of molecular orientation, but with broadside attack small impact parameter collisions could lead to formation of XeI*, as indicated by the crosshatched area in Fig. 8(a). In our experiment this would result in a decrease in chemiluminescence signal, since the detection efficiency was lower for XeI* than for XeBr*. The XeI*/XeBr* ratio would be largest for approach perpendicular to the plane of rotation [Fig. 6(a)], leading to a minimum in the signal as observed.

C. Model II: Orientation dependence of the electron transfer cross section to surface II

Consider an incoming trajectory that passes R_c(I) diabatically to reach R_c(II). The angle between the intermolecular axis and the line that connects the approaching atom with the center of mass of the molecule changes continuously during the trajectory. However, to simplify the discussion, we will consider the potentials for values (α) of this angle at the curve crossing distance R_c(II). The reason for this simplification is that the relevant part of the trajectory is at distances close to R_c(II), and therefore at an angle close to α.

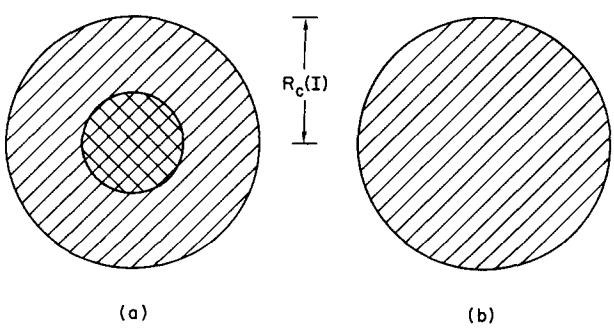

FIG. 8. Schematic reaction cross sections from model I. (a) corresponds to a perpendicular approach geometry; and (b) corresponds to a headon approach geometry. For the perpendicular approach small impact parameter collisions lead to XeI* formation, indicated by the cross hatched area.

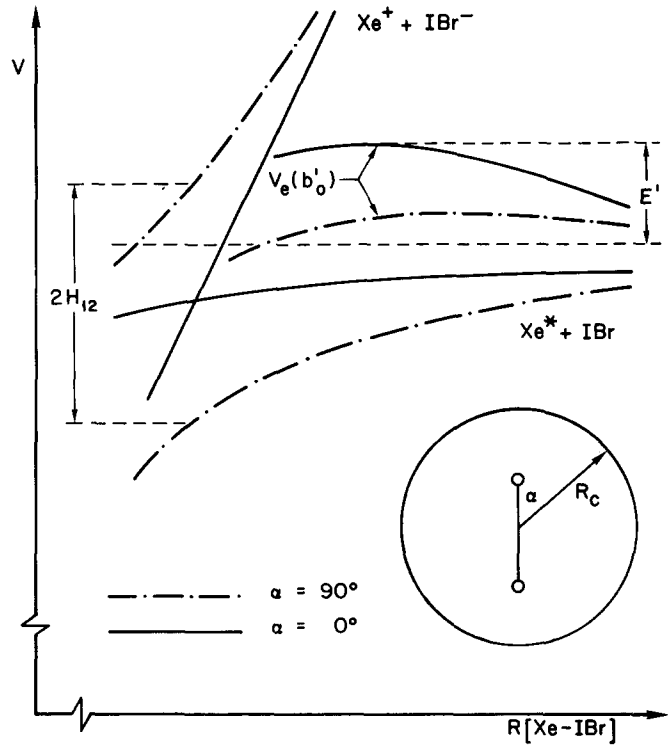

FIG. 9. Schematic diagram of the Xe–IBr potential energy curves near R_c(II) for different approach geometries. The potentials for Xe* + IBr and $Xe^+ + IBr^-$ are shown for $\alpha = 0°$ and $\alpha = 90°$. Examples of Xe* + IBr effective potentials are also shown for $\alpha = 0°$ and $\alpha = 90°$. The effective potential $V_e = V + V_c$, where $V_c = Eb^2/R^2$ is the centrifugal potential. The examples are shown for $V_e(b'_0)$, where b'_0 is taken to be the orbiting impact parameter for the Xe* + IBr $\alpha = 0°$ potential and relative kinetic energy E'. Since the $\alpha = 90°$ potential is below the $\alpha = 0°$ potential, the barrier in the corresponding V_e is also lower. The result is that for any given E' the orbiting impact parameter will be larger for $\alpha = 90°$ than for $\alpha = 0°$, giving a larger close collision cross section and larger corresponding reaction cross section.

It has been shown by Grice and Herschbach[25] that for these types of reactions at thermal energies, the cross section for reaching the crossing point is controlled by the orbiting mechanism, i.e., there is a centrifugal barrier just outside R_c that can only be passed by trajectories with an impact parameter smaller than the orbiting impact parameter b_0. For $\alpha = 0°$ H_{12} is zero, while for $\alpha = 90°$ it has its maximum value. In the latter case the adiabatic potential is more attractive, giving a larger orbiting impact parameter b_0. This is illustrated in Fig. 9. Therefore, b_0 is a function of the angle α, e.g., $b_0(90°)$ is of the order of 9 Å, and $b_0(0°)$ is of the order of 6 Å at the collision used in this work (40 meV).

We first consider atoms colliding with nonrotating molecules. Figure 10(a) shows the situation for the case when the intermolecular axis lies along the x axis and $\bar{v}$ is parallel to the x axis. The molecule is surrounded by a sphere of radius R_c(II). Most large impact parameter trajectories approach R_c with large values of α, for which $P_c = 1$. Since α is close to 90°, the orbiting impact parameter is close to the maximum value $b_0(90)$. Only trajectories with very small impact parameters

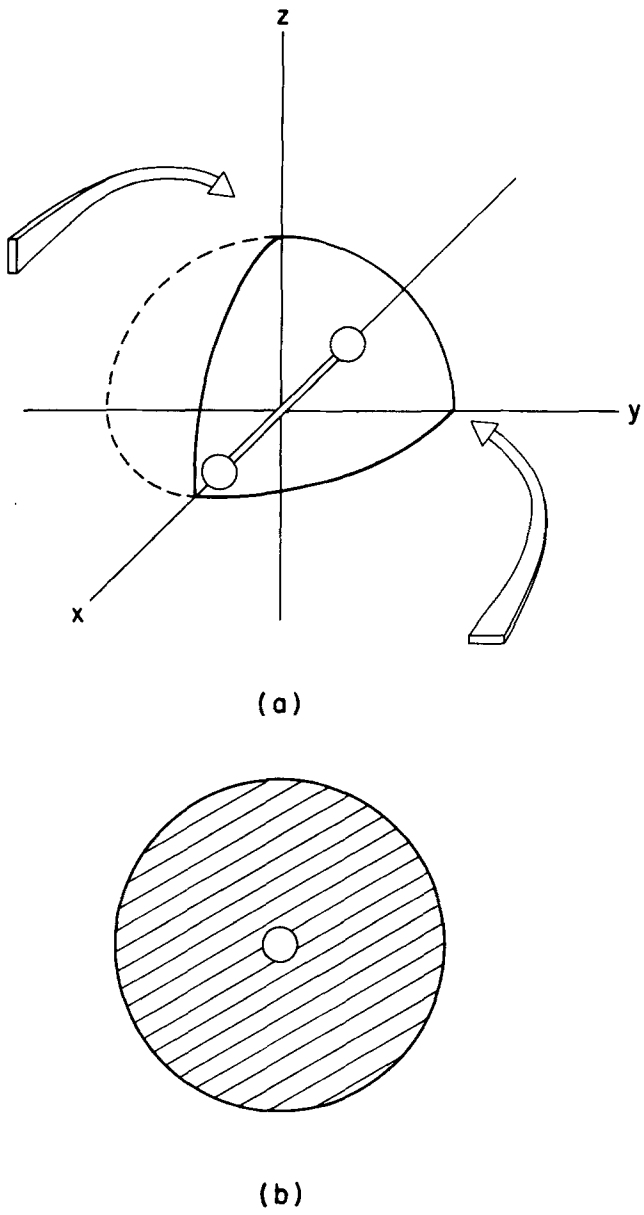

FIG. 10. Schematic reaction cross section from model II. (a) The intermolecular axis is along the x axis, and the relative velocity vector $\bar{v}$ is parallel to the x axis. Two large impact parameter trajectories are sketched, one in the xz plane and one in the xy plane; and (b) reactive cross section (projected on the yz plane).

will not lead to reaction, since P_c vanishes near $\alpha = 0$. As shown in Fig. 10(b), the reactive cross section is equal to the maximum orbiting cross section except for a small region in the middle where $P_c \to 0$.

The situation when the intermolecular axis is perpendicular to $\bar{v}$ is illustrated in Fig. 11(a). Large impact parameter trajectories in the xy plane approach R_c with large values of α, again giving orbiting impact parameters close to $b_0(90°)$. On the other hand, large impact parameter trajectories in the xz plane approach R_c with α close to 0°, and in that case the orbiting impact parameter is close to $b_0(0°)$. Therefore, the maximum reactive impact parameter is much smaller for trajectories in the xz plane than for trajectories in the xy plane. The resulting cross section is shown in Fig. 11(b).

We can now understand the results of Fig. 5 by applying the conclusions of Figs. 9 and 10 regarding the reaction cross sections for nonrotating molecules to the distributions of rotating molecules shown in Fig. 6. For the case of Fig. 6(a), the molecular axis is always perpendicular to the relative velocity vector, giving the reactive cross section of Fig. 11(b). For the case of Fig. 6(b) all angles with respect to the relative velocity vector are equally likely, causing the reaction cross section to vary from that of Fig. 10(b) to that of Fig. 11(b). Therefore, the reaction cross section is expected to be largest when Xe* approaches parallel to the plane of rotation of the IBr and smallest when Xe* approaches

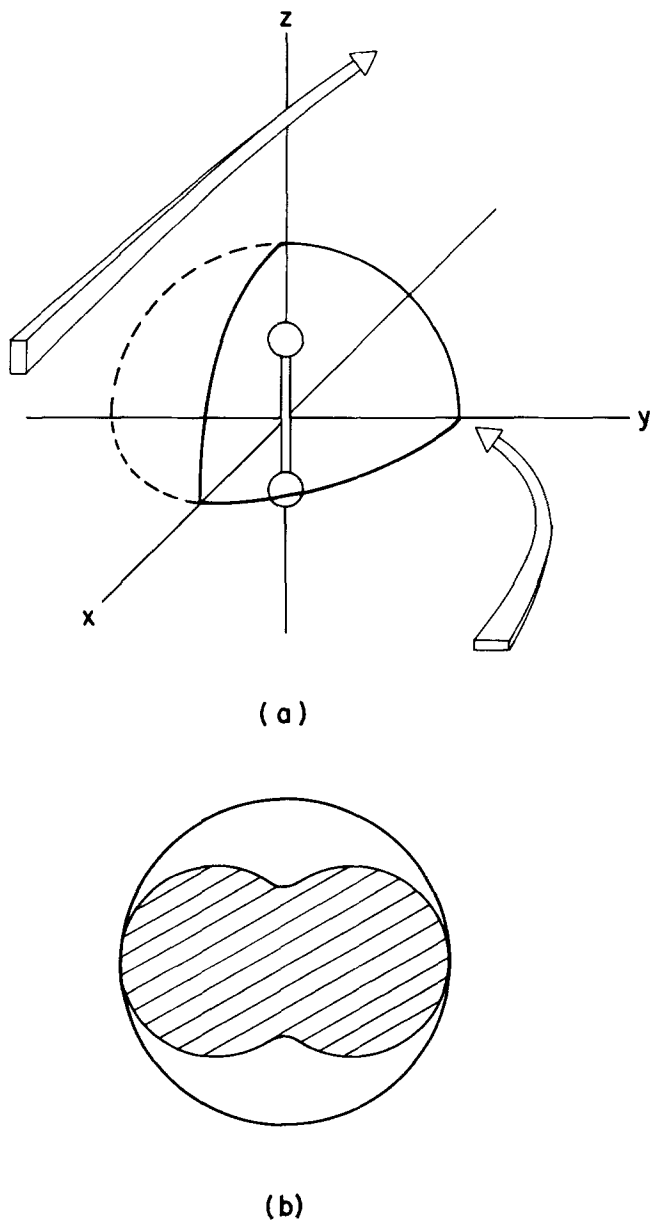

FIG. 11. Same as Fig. 10, but with the intermolecular axis along the z axis, perpendicular to the relative velocity vector.

perpendicular to the plane of rotation, as found in the results of Fig. 5.

CONCLUSION

In this paper we have described a new technique that allows information to be obtained about anisotropies of potentials that play a role in many collision processes. In general, dipole excitation offers the possibility of preparing targets of spatially polarized molecules for collision experiments. Excitation to a dissociative state makes it possible to obtain polarized ground state molecules rather than polarized excited states. With this method very sharp polarizations can be obtained, provided that the transition is saturated. Absorption cross sections for bound-free molecular transitions are usually of the order of 10^{-19} cm^2. Unfortunately, this means that high laser powers are required that can only be provided with pulsed lasers, with their inherent low duty factor. An improvement over the experimental setup described here would be the use of a pulsed nozzle molecular beam, which would provide higher target beam number densities. In future experiments an attempt should be made to obtain a uniform laser profile, so that the average target polarization can be accurately evaluated. It should also be possible to monitor the degree of polarization of the ground state target molecules using polarized laser induced fluorescence.

We conclude from this spatial polarization experiment on Xe*/IBr that the ionic surface correlating with the excited $IBr^-(^2\Pi)$ state is important in the excimer formation reaction. We have discussed two reaction models which can explain our results, both involving anisotropies in this excited state potential surface.

ACKNOWLEDGMENTS

The authors thank B. Kirtman, E. Gislason, and K. Gillen for helpful discussions, and D. Cannell for the loan of detection electronics. Support of the U.S. Department of Energy Office of Basic Energy Sciences (Grant DE-AMO3-76SF00034) is gratefully acknowledged. This work was also supported in part by the San Francisco Laser Center, a National Science Foundation Regional Instrumentation Facility, NSF Grant No. CHE79-16250, awarded to the University of California at Berkeley in collaboration with Stanford University.

[1] P. R. Brooks and E. M. Jones, J. Chem. Phys. **45**, 3449 (1966), R. J. Beuler, Jr., R. B. Bernstein, and K. H. Kramer, J. Am. Chem. Soc. **88**, 5331 (1966), R. J. Beuler, Jr. and R. B. Bernstein, J. Chem. Phys. **51**, 5305 (1969); D. van den Ende and S. Stolte, Chem. Phys. Lett. **76**, 13 (1980).
[2] C. Rettner and R. N. Zare, J. Chem. Phys. **75**, 3636 (1981).
[3] Z. Karny, R. C. Estler, and R. N. Zare, J. Chem. Phys. **69**, 5199 (1978).
[4] E. W. Rothe, F. Ranjbar, and D. Sinha, Chem. Phys. Lett. **78**, 16 (1981).
[5] R. N. Zare, Mol. Photochem. **4**, 1 (1972).
[6] R. Bersohn and S. H. Lin, Adv. Chem. Phys. **16**, 67 (1969).
[7] J. H. Ling and K. R. Wilson, J. Chem. Phys. **65**, 881 (1976).
[8] M. S. de Vries, V. I. Srdanov, C. P. Hanrahan, and R. M. Martin, J. Chem. Phys. **77**, 2688 (1982).
[9] M. S. de Vries, N. J. A. van Veen, M. Hutchinson, and A. E. de Vries, Chem. Phys. **51**, 159 (1980).
[10] D. J. Seery and D. Britton, J. Phys. Chem. **68**, 2263 (1964).
[11] D. W. Setser, T. D. Dreiling, H. C. Brashears, Jr., and J. H. Kolts, Discuss. Faraday Soc. **67**, 255 (1979).
[12] D. J. Auerbach, M. M. Hubers, A. P. M. Baede, and J. Los, Chem. Phys. **2**, 107 (1973).
[13] E. A. Gislason and J. G. Sachs, J. Chem. Phys. **62**, 2678 (1975).
[14] S. K. Searles and G. A. Hart, Appl. Phys. Lett. **28**, 24 (1976).
[15] J. E. Velazco and D. W. Setser, J. Chem. Phys. **62**, 1990 (1975).
[16] C. T. Rettner and J. P. Simons, Chem. Phys. Lett. **59**, 178 (1978).
[17] *The Physical Basis of Polarized Emission*, edited by P. P. Feovilof (Consultation Bureau of New York, 1961).
[18] R. J. Hennessy and J. P. Simons, Chem. Phys. Lett. **75**, 43 (1980).
[19] J. Los and A. W. Kleyn, in *The Alkali Halide Vapors*, edited by P. Davidovits and D. McFadden (Academic, New York, 1978).
[20] A. P. Hickman and K. T. Gillen, J. Chem. Phys. **73**, 3672 (1980).
[21] R. W. Anderson, Ph.D. thesis, Harvard University (1968).
[22] R. E. Olson, F. T. Smith, and E. Bauer, Appl. Opt. **10**, 1848 (1971).
[23] J. A. Aten, G. E. H. Lanting, and J. Los, Chem. Phys. **19**, 241 (1976).
[24] J. A. Aten and J. Los, Chem. Phys. **25**, 47 (1977).
[25] R. Grice and D. R. Herschbach, Mol. Phys. **27**, 159 (1974).
[26] G. H. Kwei and D. R. Herschbach, J. Chem. Phys. **51**, 1742 (1969).
[27] G. G. Balin-Kurti, Mol. Phys. **25**, 393 (1973).
[28] E. A. Gislason, in *The Alkali Halide Vapors*, edited by P. Davidovits and D. McFadden (Academic, New York, 1978).